PAPER

Tunable surface plasmon resonance in laser-induced plasma spheroids

To cite this article: Roberto A Colón Quiñones *et al* 2021 *Plasma Sources Sci. Technol.* **30** 045010

IOP Publishing Plasma Sources Science and Technology
Plasma Sources Sci. Technol. **30** (2021) 045010 (6pp) https://doi.org/10.1088/1361-6595/abc5a2

Tunable surface plasmon resonance in laser-induced plasma spheroids

Roberto A Colón Quiñones[1,2,*], **Thomas Carlton Underwood**[2,3] and **Mark A Cappelli**[3]

[1] Lawrence Livermore National Laboratory, Livermore, CA 94550, United States of America
[2] Stanford University, Stanford, CA 94305, United States of America
[3] University of Texas at Austin, Austin, TX 78712, United States of America

E-mail: racolon@alumni.stanford.edu

Received 7 June 2020, revised 11 September 2020
Accepted for publication 28 October 2020
Published 14 April 2021

Abstract

We present a study of the Ku-band tunability of the surface plasmon response of a gaseous plasma resonator generated by laser-induced gas breakdown. Tuning is achieved by varying gas pressure and laser pulse energy. Microwave scattering characteristics of the plasma resonator are obtained using an experimental configuration in which a waveguide is loaded with a single plasma element. Optical imaging of the laser plasma is used to characterize the time-dependent plasma size. Complex transmission waveforms are attributed to the dynamic expansion of the plasma, resulting first in a sweep through the principle Mie resonance, followed by strong reflection of the incident wave due to bulk plasma loading as the plasma expands to significantly fill the waveguide. The described resonator has the potential to be used in an all-plasma metamaterial with tunable opacity and resonance frequency.

Keywords: metamaterial, laser-induced plasma, surface plasmon

(Some figures may appear in colour only in the online journal)

1. Introduction

Metamaterials (MTMs) are artificial materials engineered to exhibit electromagnetic (EM) properties not readily found in nature [1]. The resonantly active elements in MTMs, and their spacing, are designed to create a homogeneous medium with engineered EM properties. Such a medium is achieved when the spacing between the constituent elements is smaller than a quarter of the guided wavelength [2]. The ability to create MTMs with exotic effective properties has lead to the formation of the very active field of transformation optics where MTMs of spatially varying refractive indexes are used to steer EM waves in unusual ways to achieve phenomena such as negative refraction, perfect lensing, and optical cloaking [3].

In recent years, a significant portion of research in this field has focused on exploring the tunability of these phenomena [4]. One class of potentially tunable elements that has been investigated are gaseous plasmas, which can be incorporated into more traditional MTMs to form composite periodic structures with tunable features [5, 6]. The tunability of these structures stems from the dispersive nature of plasmas arising from their variable electron density (n_e) and electron momentum transfer collision frequency (ν). These two plasma properties are in turn controlled by the energy invested by the ionizing source and the pressure/composition of the gas.

The majority of past research related to plasma MTMs has focused mainly on the development of composites that integrate plasmas into metallic resonant structures [7–17] or into dielectric resonator arrays [18–20]. Waveguiding MTM structures composed exclusively of plasma filaments have also been proposed [21], but have yet to be realized experimentally. In a recent publication [22], we showed that an all-plasma MTM could be potential achieved through an array of laser-induced plasma (LIP) spheroids, which are individually generated by tightly focusing the fundamental output from a pulsed, high-energy laser through a lens and into a gas [23, 24]. We found that given their plasmonic nature and ellipsoidal geometry, surface plasmon resonances could be excited

* Author to whom any correspondence should be addressed.

in these sub-wavelength plasmas when they are smaller than a quarter of the guided wavelength and n_e is below critical. The sub-wavelength spheroid [25, 26] with near-uniform n_e achieved after electron concentrations at the edge of the plasma have decayed [24], interacts with incoming radiation through excitation of low-order, electric-dipole resonances similar to those seen in metallic spheres [27]. These electric-dipoles are induced by the restoring force of the plasma boundary on the oscillating electrons. In this paper, we investigate the effect of varying the laser pulse energy and working gas pressure used to generate these LIPs on their scattering response.

The results presented here build on the previously described work by showing that for both increasing amounts of laser pulse energy and working gas pressure, the LIP becomes larger and in turn has a stronger scattering response as long as the LIP is smaller than a quarter of the guided wavelength. Once the plasma size exceeds this quarter wavelength limit [2], the plasma acts increasingly more like a bulk plasma, i.e., a semi-infinite plasma slab. The observed tunable properties demonstrate that when used as meta-atoms in an all-plasma MTM [1], these resonators afford the user the ability to tune the MTM's fill fraction and, in turn, its radiative opacity at resonance. The results also demonstrate the potential to generate plasma surfaces that can operate in both an MTM and a bulk plasma regime, depending on the choice of laser energy and gas pressure. Potential applications of such tunable surfaces include, but are not limited to, highly-tunable reflective surfaces and negative-index mediums with fully three-dimensional structural flexibility. These MTMs are particularly suited for high-power microwave applications where the small gaps in more traditional, metallic MTMs short [9, 12, 13] and remote generation is advantageous. Moreover, the plasma densities ($n_e \leqslant 10^{25}$ m^{-3}) [24] and dimensions (size $\geqslant 10$ μm) [26] achieved in these resonators translate to resonance frequencies as high as a few THz, making these MTMs potentially suitable for applications in the elusive THz gap.

2. Waveguide scattering measurements

A simplified schematic of the experimental setup used for the microwave scattering measurements can be found in figure 1. The collimated output pulse generated by a Q-switched Nd:YAG laser (wavelength: 1064 nm, repetition rate: 10 Hz, pulse duration: 10 ns, beam diameter: 10 mm) was focused through a plano-convex lens (diameter: 30 mm, focal length: 40 mm) to produce a plasma spheroid with major axis oriented parallel to the incident electric field inside a Ku band, WR62 waveguide. The Ku band (12–18 GHz) was selected as the frequency regime of interest due its relatively large bandwidth and ease of obtaining experimental equipment. The wavelengths associated with this regime also allowed us to probe the surface plasmon resonance of the millimeter size LIPs generated by our laser under conditions similar to those in reference [22]. The plasma was generated in the same 93%N_2/7%H_2 gas mixture used in reference [22] for consistency. The plasma was generated through a 4 mm diameter hole on the waveguide and any light not absorbed at the focal spot was transmitted through an identical hole located

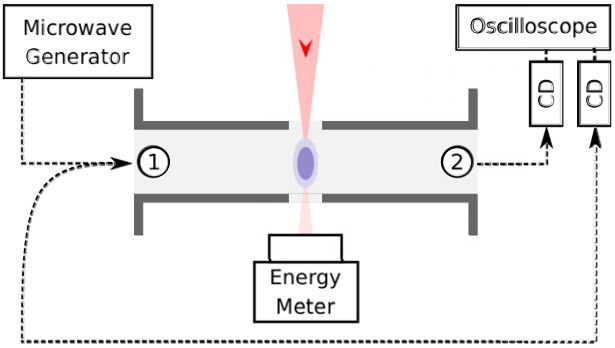

Figure 1. Simplified schematic of the experimental setup used for Ku band microwave scattering measurements.

coaxially and on the opposite waveguide wall. This transmitted light was then measured by an Ophir Photonics PE50BF-DIF-C energy meter to determine the energy absorbed by the LIP. The incident continuous microwave signal was generated by an HP 83732A signal generator and sent through the input port of a WR62 waveguide coupler connected to port 1. The transmitted power was set to 10 dBm as this was the maximum level of stable output power provided by the generator and lower output powers led to lower signal-to-noise ratios. The reflected signal from the waveguide coupler and transmitted signal at port 2 were detected by Krytar 303SK crystal detectors and recorded through a Rohde and Schwarz, 1 GHz RTE1104 oscilloscope, which was synced with the laser Q-switch trigger. This allowed us to record the reflection/transmission of the system during the plasma's lifetime. The nanosecond rise time afforded by these detectors and comparable oscilloscope resolution allowed us to detect the time evolution of the scattered microwave signal from this short-lived plasma with high temporal resolution.

The waveguide was placed in a vacuum chamber capable of supporting gas mixtures over a range of pressures, with optical ports for laser access and plasma imaging. Results are presented for the case where the N_2 gas mix ambient pressure is kept constant at $P = 20$ Torr while the laser pulse energy is varied in the range 0.2 J $< E <$ 1 J. Similarly, results are presented for the case where the laser pulse energy is kept constant at $E = 0.2$ J while the ambient gas pressure is varied in the range 10 Torr $< P <$ 100 Torr. These results demonstrate a tunable range of the LIP's surface plasmon resonance for conditions spanning an order of magnitude in laser energy and gas pressure.

2.1. Constant P, variable E

In this section, we investigate how increasing the laser pulse energy affects the LIP and, in turn, the value of its resonance frequency (f_0). The value of E was varied in the range 0.2 J $< E <$ 1 J while keeping all other laser, optic, and gas conditions described at the beginning of section 2 constant. The microwave transmission data measured at port 2 was normalized by the microwave signal received at this port when the plasma was off to obtain the transmittance (T) due to the plasma. Similarly, the reflection data measured at port 1 was

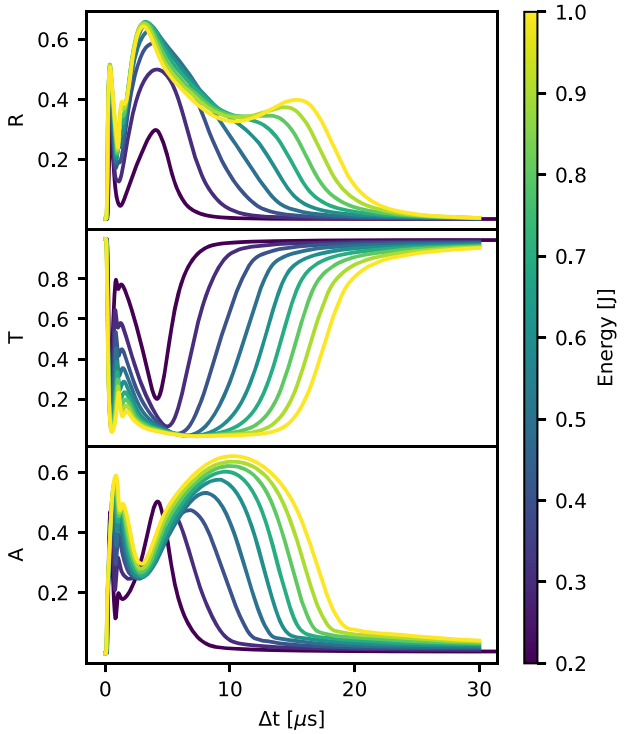

Figure 2. Plots of the time evolution of reflectance (R), transmittance (T), and absorbance (A) at $f = 15$ GHz for a WR62 waveguide embedded with an LIP generated at $P \approx 20$ Torr and 0.2 J $< E <$ 1 J.

normalized by the microwave signal received at this port after placing a copper plate at the center of the waveguide in place of the LIP in order to obtain the reflectance (R) due to the plasma. Given this normalization, the absorbance (A) of the plasma is therefore obtained from an energy balance, i.e., $A = 1 - R - T$. The time evolution of R, T, and A obtained from this two-port waveguide experiment can be found in figure 2. Only results at a microwave frequency of $f = 15$ GHz are presented in order to avoid clutter and focus solely on the effects of varying E. This frequency was simply chosen because it is at the center of the Ku band. The data is presented as a function of Δt, which was the delay time between the laser Q-switch trigger and the time the measurement was taken. Similar to the results on reference [22], there are two noticeable reflection peaks and corresponding transmission dips. The first is due to a wave cutoff effect from a layer of weakly ionized plasma surrounding the hot plasma kernel that fills the microwave cavity at early times. This layer, referred to in the literature as an ionization aureole [24], is formed as a result of photoionization of the gas by short-wavelength radiation emitted by the central core of the LIP. The second peak is due to a surface plasmon resonance effect. The sub-wavelength spheroid [25, 26] with near-uniform n_e achieved after electron concentrations at the edge of the plasma have decayed [24], interacts with incoming radiation through excitation of low-order, electric-dipole resonances similar to those seen in metallic spheres [27]. These electric-dipoles are induced by the restoring force of the plasma boundary on the oscillating electrons.

As E increases, this behavior continues up to about $E \approx$ 0.4 J with an increase in peak R and corresponding decrease

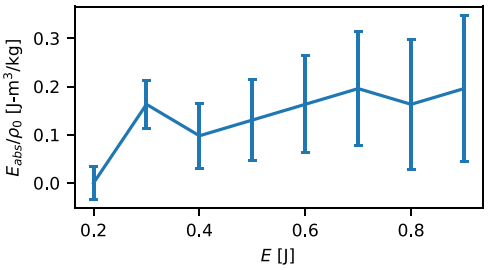

Figure 3. Plot of E_{abs}/ρ_0 vs E demonstrating an increase in E_{abs}/ρ_0 with increasing E.

in minimum T with increasing E near f_0. This increase in R and decrease in T can be attributed to an increase in plasma size with increasing E. An increase in plasma size will lead to a larger fill fraction of the LIP with respect to the waveguide cross-section, which in turn will lead to a greater amount of backward-scatter, i.e., reflection, and a corresponding reduction in transmission. For $E > 0.4$ J, the resonance R peak appears to hit a maximum followed by an expansion of the curve's width in time and a subsequent decrease in R near the center of the curve with increasing E. Similarly, the corresponding transmission dip appears to hit a minimum followed by an expansion of the curve's width in time. Finally, the corresponding A plot shows a gradual increase in its peak value near resonance. All of these results point to the fact that an increase in E leads to an increase in the plasma size. The best possible explanation for the trends observed in figure 2 is that for $E <$ 0.4 J, the plasma size is $< \lambda/4$, i.e., inside the Mie regime, and for $E > 0.4$ J, the plasma size exceeds this small-particle limit and starts to behave more like a bulk plasma.

The hypothesis made in the previous paragraph can be verified by looking at the physical mechanisms governing the initial expansion of the LIP. The size achieved by an LIP at the end of the laser pulse is primarily governed by the interaction of the laser radiation with a detonation shockwave formed due to intense heating from the laser at the focal point [28]. The LIP size is then determined by the velocity of the shockwave, with a larger velocity leading to a faster plasma expansion, and therefore, a larger plasma size. From the literature [29], we find that by assuming an ideal gas and applying the Chapman–Jouguet theory, the velocity of this detonation shockwave along a constant area channel of radius r can be approximated by

$$v = \left[\frac{2(\gamma^2 - 1)P_{abs}}{\pi r^2 \rho_0}\right]^{\frac{1}{3}}, \quad (1)$$

where γ is the gas specific-heat ratio, P_{abs} is the laser pulse power absorbed by the gas, r is the beam waist of the focused laser beam, and ρ_0 is the initial gas density. This equation has been validated through experiments by several authors [28, 29]. For the case of an optically thin gas (such as our N_2/H_2 mix at low pressures) where not all of the incident energy is absorbed, P_{abs} can be expressed as [29]

$$P_{abs} = P_{inc} k y, \quad (2)$$

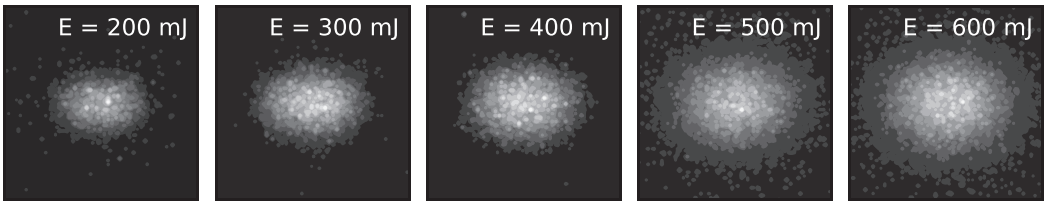

Figure 4. Sequence of 8.25 mm × 8.25 mm images showing the evolution of the LIP's broadband emission, i.e., it is size, with increasing laser pulse energy.

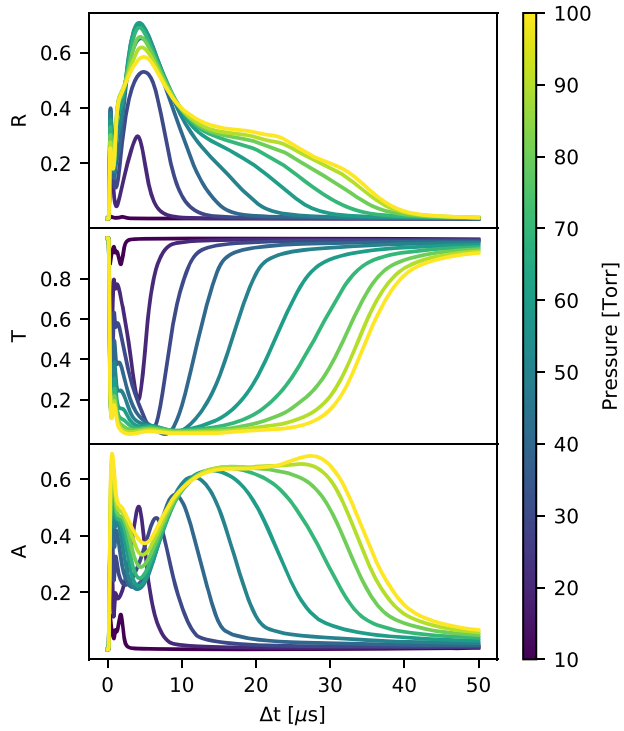

Figure 5. Plots of the time evolution of reflectance (R), transmittance (T), and absorbance (A) at $f = 15$ GHz for a WR62 waveguide embedded with an LIP generated with $E \approx 200$ mJ and 10 Torr $< P <$ 100 Torr.

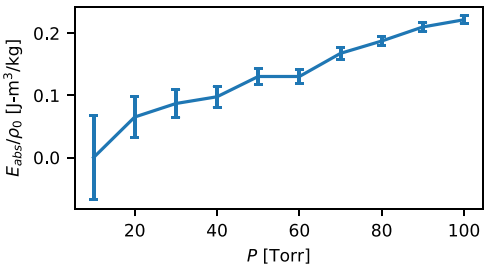

Figure 6. Plot of E_{abs}/ρ_0 vs P demonstrating an increase in E_{abs}/ρ_0 with increasing P.

where P_{inc} is the incident laser power, k is the gas inverse bremsstrahlung absorption coefficient, and y is the gas effective absorption depth. Since the gas and focusing optics used in our experiments are fixed, equation (1) tells us that the detonation wave velocity will increase/decrease with increasing/decreasing P_{abs}/ρ_0. Since the laser pulse length in these experiments is also fixed, we can simplify this ratio one step further by writing it as E_{abs}/ρ_0, where E_{abs} is the energy absorbed by the working gas.

For the case of constant P and variable E, ρ_0 is constant and this ratio will increase through E_{abs} leading to an increase in detonation velocity, which in turn will lead to higher expansion velocities and thus a larger plasma radius. Figure 3 shows the results of energy absorption measurements that were carried out in order to confirm this trend through a plot of E_{abs}/ρ_0 vs E. At these low pressure conditions, the energy absorbed at the focal spot ranged from ∼1 mJ at $E = 0.2$ J to ∼7 mJ at $E = 1$ J. As we can see, this increasing trend leads to an increase in the ratio of E_{abs}/ρ_0 with increasing laser pulse energy, which leads to an increase in the detonation velocity and in turn an overall increase in the size of the LIP. The error bars in the figure are associated with the $\pm 2\%$ shot-to-shot drift in the measured laser pulse energy that went into calculating E_{abs}.

In an effort to provide further confirmation for the hypothesis that the plasma expands beyond the Mie regime after a certain energy threshold, broadband optical emission images of the plasma were captured in order to look at the evolution of plasma size with increasing E. The images were captured by an intensified CCD camera, which was triggered simultaneously with the laser Q-switch and gated to a 150 ns exposure. The gated images were captured for energies in the range 0.2 J $< E <$ 0.6 J. Energies beyond this range were beyond the apparent transition between the surface plasmon and bulk plasma regime observed in figure 2 and were therefore not considered. All images were captured at the time where resonance occurs at 15 GHz, i.e., at the Δt of least transmission on figure 2, as this was the time of interest. The captured sequence of 8.25 mm × 8.25 mm images can be found on figure 4. Given that these images were primarily generated by light emitted through recombination radiation and excitation of neutral species throughout the plasma [30], the images provided a good estimate for the geometry and size of the resonators. As predicted, this sequence of images shows that the size of the plasma increases with increasing E. At the previously described threshold of $E = 0.4$ J, the major axis of the LIP is ∼5 mm in length. This length places the LIP just at the Mie regime limit of $\lambda/4$, which is ∼5 mm for the 15 GHz microwave signal used to obtain the results on figure 2. For energies slightly above this threshold, i.e., $E = 0.5$ J, the major axis of the LIP is closer to ∼6.5 mm, which is clearly above the Mie regime limit. Hence, these images show that the changes in the microwave scattering signal on figure 2 are mostly driven by resonator size effects.

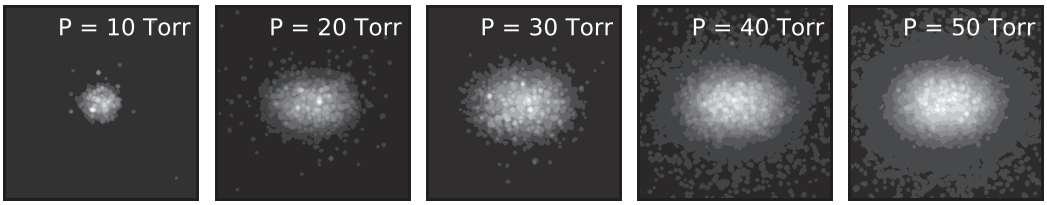

Figure 7. Sequence of 8.25 mm × 8.25 mm images showing the evolution of the LIP's broadband emission, i.e., it is size, with increasing gas pressure.

2.2. Constant E, variable P

In this section, we investigate how increasing the working gas pressure affects the LIP and in turn the value of f_0. The value of P was varied in the range 10 Torr $< P <$ 100 Torr while keeping all other laser, optic, and gas conditions described at the beginning of section 2 constant. The same two-port, WR62 waveguide setup described in section 2 and shown in figure 1 was used.

The time evolution of the R, T, and A obtained from this two-port waveguide experiment can be found in figure 5. Again, only results at $f = 15$ GHz are presented in order to avoid clutter and focus solely on the effects of varying P. As before, the data is presented as a function of Δt, which was the delay time between the laser Q-switch trigger and the time the measurement was taken. As expected, for pressures comparable to the ∼20 Torr used to obtain the results on figure 2, there are two noticeable reflection peaks and corresponding transmission dips. As P increases, this behavior continues up to about $P \approx 40$ Torr with an increase in peak R and corresponding decrease in minimum T with increasing P near f_0. Similar to the variable E results of the previous section, this increase in R and decrease in T could potentially be attributed to an increase in plasma size with increasing P. An increase in plasma size will lead to a larger fill fraction of the LIP with respect to the waveguide cross-section, which in turn will lead to a greater amount of backward-scatter, i.e., reflection, and a corresponding reduction in transmission. For $P >$ 40 Torr, the resonance R peak appears to hit a maximum followed by an expansion of the curve's width in time and a gradual decrease in the peak R value. Similarly, the corresponding transmission dip appears to hit a minimum followed by an expansion of the curve's width in time. Finally, the corresponding A plot shows a gradual increase in its peak value near resonance. As in the previous section, all of these results point to the fact that an increase in P leads to an increase in the plasma size. As we already know at this point, the best possible explanation for the trends observed in figure 5 is that for $P <$ 40 Torr, the plasma size is $< \lambda/4$, i.e., inside the Mie regime, and for $P >$ 40 Torr, the plasma size exceeds this small-particle limit and starts to behave more like a bulk plasma.

For the case of constant E and variable P, ρ_0 is expected to increase through P, assuming an ideal gas, and E_{abs} is expected to increase as well given the increase in absorption cross-section associated with an increase in the gas density. An increase in E_{abs} exceeding the increase in ρ_0 will lead to an increase in the detonation velocity of equation (1), which in turn will lead to a larger plasma. Figure 6 shows the results of energy absorption measurements that were carried out in order to confirm this trend through a plot of E_{abs}/ρ_0 vs P. As we can see, the ratio of E_{abs}/ρ_0 increases with increasing laser pulse energy, which leads to an increase in the detonation velocity and in turn an overall increase in the size of the LIP. Similar to figure 3, the error bars in the figure are associated with the $\pm 2\%$ shot-to-shot drift in the measured laser pulse energy that went into calculating E_{abs}. Comparing these results to those of figure 3 we see that the range of E_{abs}/ρ_0 values observed is almost the same for both the variable E and the variable P case. This would explain the similarity between the results on figures 2 and 5. One noticeable difference between the figures is a steeper decrease in peak R and increase in T for higher values of P in figure 5, which could point to the fact that not only is the increased plasma size leading to a reduction in the peak reflection, but also the effect of increased electron–neutral collision losses, with an increase in pressure. As explained in reference [22], the electron–neutral collision frequency (ν) in the LIP is proportional to the pressure and its value must be limited to be a small fraction of f_0 to ensure that electrons in the LIP can oscillate freely and respond strongly to incident electric fields without being hindered by collisions with neutrals. The decrease in peak R for $P >$ 40 Torr seen in figure 5, but not in figure 2, likely points to a transition point in pressure where ν approaches and subsequently exceeds f_0 with increasing P.

In an effort to provide further confirmation for the hypothesis that the plasma expands beyond the Mie regime after a certain pressure threshold, broadband optical emission images of the plasma were used to look at the evolution of plasma size with increasing P. The same experimental setup used for the images on figure 4 and described in reference [22] was used here. The 150 ns gated images were captured for pressures in the range 10 Torr $< P <$ 50 Torr. Pressures beyond this range were beyond the apparent transition between the surface plasmon and bulk plasma regime observed in figure 5 and were therefore not considered. All images were captured at the time where resonance occurs at 15 GHz, i.e., at the Δt of least transmission on figure 5, as this was the time of interest. The captured sequence of 8.25 mm × 8.25 mm images can be found on figure 7. As predicted, this sequence of images shows that the size of the plasma increases with increasing P. At the previously described threshold of $P = 40$ Torr, the major axis of the LIP is ∼4.5 mm in length. This length places the

LIP just below the Mie regime limit of $\lambda/4$, which is ∼5 mm for the 15 GHz microwave signal used to obtain the results on figure 5. For pressures slightly above this threshold, i.e., $P = 50$ Torr, the major axis of the LIP is closer to ∼5 mm, which is at the Mie regime limit. Even though this plasma does not appear to be much larger than the Mie regime limit, it is possible that the onset of distortion effects on figure 5 is not only due to size, but also due to the electron–neutral collision losses previously discussed. Hence, even though these images do not tell the whole story, they do provide further evidence to the hypothesis that the changes in the microwave scattering signal on figure 5 are in part due to resonator size effects.

3. Summary

In summary, we described experimental efforts to prove the existence of a surface plasmon scattering effect occurring during the decay phase of sub-wavelength LIPs. Results were presented showing the effect of varying working gas pressure and laser pulse energy on the surface plasmon scattering resonance of the LIP. The variable energy results showed that, for the range of energies considered, the LIP grew in size with increasing energy due to a corresponding increase in the expansion velocity of the plasma at early times. This increase in resonator size led to an increase in peak R and corresponding decrease in minimum T at resonance for $h < \lambda/4$. As the resonator increased beyond this Mie regime limit, the R, T, and A results appeared to look more like those expected from a bulk plasma. Similar trends were observed for the variable pressure case with the only difference being that a decrease in peak R and corresponding increase in minimum T were observed before the plasma size reached the Mie regime limit. This effect was attributed to additional scattering losses associated with the increase in electron–neutral collision losses tied to the increase in gas pressure. These tunable properties demonstrate that when used as meta-atoms in an all-plasma MTM, these resonators afford the user the ability to tune the MTM's fill fraction and, in turn, it is opacity at resonance. The results also demonstrate the potential to generate plasma surfaces that can operate in both an MTM and bulk plasma regime, depending on the choice of laser energy and gas pressure.

Acknowledgments

This work was supported by the Air Force Office of Scientific Research under Award No. FA9550-14-10317. R Colón Quiñones and T Underwood gratefully acknowledge the financial support of the National Defense Science and Engineering Graduate Fellowship Program.

ORCID iDs

Roberto A Colón Quiñones https://orcid.org/0000-0002-6944-7199
Mark A Cappelli https://orcid.org/0000-0003-3093-3357

References

[1] Smith D R, Pendry J B and Wiltshire M C 2004 *Science* **305** 788–92
[2] Caloz C and Itoh T 2005 *Electromagnetic Metamaterials* (*Transmission Line Theory and Microwave Applications*) (New York: Wiley)
[3] Chen H, Chan C T and Sheng P 2010 *Nat. Mater.* **9** 387–96
[4] Zheludev N I and Kivshar Y S 2012 *Nat. Mater.* **11** 917–24
[5] Sakai O and Tachibana K 2012 *Plasma Sources Sci. Technol.* **21** 013001
[6] Adamovich I *et al* 2017 *J. Phys. D: Appl. Phys.* **50** 323001
[7] Lee D-S, Sakai O and Tachibana K 2009 *Jpn. J. Appl. Phys.* **48** 062004
[8] Nakamura Y, Iwai A and Sakai O 2014 *Plasma Sources Sci. Technol.* **23** 064009
[9] Singh P K, Hopwood J and Sonkusale S 2014 *Sci. Rep.* **4** 5964
[10] Liu C-H, Carrigan P, Kupczyk B J, Xiang X, Behdad N, Scharer J E and Booske J H 2015 *IEEE Trans. Plasma Sci.* **43** 4099–109
[11] Lee R, Wang B and Cappelli M A 2017 *Appl. Phys. Lett.* **111** 261105
[12] Kim H, Parsons S and Hopwood J 2018 *Plasma Sources Sci. Technol.* **27** 015010
[13] Kim H and Hopwood J 2018 *Plasma Sources Sci. Technol.* **27** 095007
[14] Matlis E H, Corke T C, Neiswander B and Hoffman A J 2018 *J. Appl. Phys.* **124** 093104
[15] Navarro R, Liard L and Sokoloff J 2019 *J. Appl. Phys.* **126** 163304
[16] Kim H and Hopwood J 2019 *Sci. Rep.* **9** 1–7
[17] Iwai A, Righetti F, Wang B, Sakai O and Cappelli M A 2020 *Phys. Plasmas* **27** 023511
[18] Cohick Z, Luo W, Perini S, Baker A, Wolfe D and Lanagan M 2016 *Appl. Phys. Express* **9** 116201
[19] Dennison S, Chapman A, Luo W, Lanagan M and Hopwood J 2016 *Plasma Sources Sci. Technol.* **25** 03LT02
[20] Fantini L, Dennison S, Kim H, Sarkarat M, Lanagan M and Hopwood J 2019 *J. Appl. Phys.* **126** 203301
[21] Kudyshev Z A, Richardson M C and Litchinitser N M 2013 *Nat. Commun.* **4** 2557
[22] Colón Quiñones R A, Underwood T C and Cappelli M A 2018 *Phys. Plasmas* **25** 113501
[23] DeMichelis C 1969 *IEEE J. Quantum Electron.* **5** 188–202
[24] Ostrovskaya G V and Zaĭdel' A N 1974 *Sov. Phys. Usp.* **16** 834–55
[25] Chen Y-L, Lewis J W L and Parigger C 2000 *J. Quant. Spectrosc. Radiat. Transfer* **67** 91–103
[26] Roskos H G, Thomson M D, Kreĭ M and Löffler T 2007 *Laser Photon. Rev.* **1** 349–68
[27] Bohren C F and Huffman D R 1998 *Absorption and Scattering of Light by Small Particles* (New York: Wiley)
[28] Ramsden S A and Savic P 1964 *Nature* **203** 1217–9
[29] Daiber J W and Thompson H 1967 *Phys. Fluids* **10** 1162–9
[30] Griem H R 1963 *Plasma Spectroscopy* (New York: McGraw-Hill)